Program

THE NINETEENTH INTERNATIONAL SYMPOSIUM ON ARTIFICIAL LIFE AND ROBOTICS

(AROB 19th 2014)

January 22– 24, 2014

B-Con Plaza, Beppu, Oita, JAPAN

International Society of Artificial Life and Robotics

Contents

1	Organization, etc.	1
2	Messages	6
3	Conference rooms	8
4	Time Table	9
5	Abstracts	
5-1	Plenary Speeches	12
5-2	Special Session	13
5-3	January 22, 2014	14
5-4	January 23, 2014	47
5-5	January 24, 2014	71
6	Author Index	84
7	Invitation for publication in Artificial Life and Robotics, Springer	90

THE NINETEENTH INTERNATIONAL SYMPOSIUM ON ARTIFICIAL LIFE AND ROBOTICS

(AROB 19th 2014)

ORGANIZED BY

International Society on Artificial Life and Robotics (ISAROB)

CO- ORGANIZED BY

The Institute of Electrical Engineers of Japan (IEEJ, Japan)
The Institute of Electronics, Information and Communication Engineers (IEICE, Japan)

CO-OPERATED BY

The Society of Instrument and Control Engineers (SICE, Japan)
The Robotics Society of Japan (RSJ, Japan)
The Institute of Systems, Control and Information Engineers (ISCIE, Japan)
IEEE Robotics and Automation Society Japan Chapter
Japan Association for Omics-baced Medicine (JSOM, Japan)

SUPPORTED BY

Oita Prefecture
Beppu City
Oita City
The Federation of Oita Chamber of Commerce and Industry
Kyodo News
JIJI PRESS OITA BUREAU
Oita Godo Shimbun Inc.
Nishinippon Shimbun
The Asahi Shimbun
THE MAINICHI NEWSPAPERS
Japan Broadcasting Corporation Oita Station
OITA BROADCASTING SYSTEM
Television Oita System
Oita Asahi Broadcasting Co., Ltd.

The Nineteenth International Symposium on Artificial Life and Robotics 2014 (AROB 19th 2014),
B-Con Plaza, Beppu, Japan, January 22-24, 2014

Computer simulations on vibration control of a flexible single-link manipulator using finite-element method

Abdul Kadir Muhammad[1,2], Shingo Okamoto[1], and Jae Hoon Lee[1]

[1]Graduate School of Science and Engineering, Ehime University, Japan

y861008b@mails.cc.ehime-u.ac.jp, okamoto.shingo.mh@ehime-u.ac.jp

[2]Center for Mechatronics and Control Systems, Department of Mechanical Engineering, State Polytechnic of Ujung Pandang, Indonesia

Abstract: The purposes of this research are to formulate the equation of motion of the system, to develop the computational codes by a finite-element method in order to perform dynamics simulations with vibration control and to propose an effective control scheme of a flexible single-link manipulator. The system used in this paper consists of an aluminum beam as a flexible link, a clamp-part, a servo motor to rotate the link and a couple of piezoelectric actuator to control vibration. Computational codes on time history responses, FFT (Fast Fourier Transform) processing and eigenvalues - eigenvectors analysis were developed to calculate the dynamic behavior of the link. Furthermore, a control scheme using the piezoelectric actuators was designed to suppress the vibration. A proportional-derivative controller was designed and demonstrated its performances. The calculated results of the controlled single-link manipulator revealed that the vibration of the flexible manipulator can be controlled effectively.

Keywords: Finite-element method, flexible manipulator, piezoelectric actuator, vibration control.

1 INTRODUCTION

Employment of flexible manipulators is recommended in the industrial applications in order to accomplish high performance requirements such as high-speed but safe operation, increasing of positioning accuracy, less weight and lower energy consumption. However, a flexible manipulator usually cannot be controlled easily because of its inheriting flexibility. Deformation of the flexible manipulator when it is operated must be considered in the control. Its controller system should deal with not only its motion but also vibration due to flexibility.

The purposes of this research are to formulate the equation of motion of the system, to develop computational codes by a finite-element method in order to perform dynamics simulation with vibration control and to propose an effective control scheme of the single link flexible manipulator. The system used in this paper consists of an aluminum beam as a flexible link, a clamp-part, a servo motor to rotate the link and a couple of piezoelectric actuator to suppress vibration. Computational codes on time history responses, FFT (Fast Fourier Transform) processing and eigenvalues - eigenvectors analysis were developed to calculate the dynamic behavior of the link validated by the experimental one. Furthermore, an end-effector that treated as a concentrate mass was introduced to demonstrate a complete flexible single-link manipulator system. Finally, a proportional-differential (PD) controller was designed to suppress the vibration. It was done by adding moments of force generated by the piezoelectric actuators to the single-link.

2 FORMULATION BY FINITE-ELEMENT METHOD

The link has been discretized by finite-elements. The finite-element has two degrees of freedom, namely the lateral deformation $v(t)$, and the rotational angle $\psi(t)$. The length, the cross-sectional area and the area moment of inertia around z-axis of every element are denoted by l_i, S_i and I_{zi} respectively. Mechanical properties of every element are denoted as Young's modulus E_i and mass density ρ_i.

2.1 Kinematics

Figure 1 shows the position vector of an arbitrary point P in the link in the global and rotating coordinate frames. Let the link as a flexible beam has a motion that is confined in the horizontal plane as shown in figure 1. The $O - XY$ frame is the global coordinate frame while $O - xy$ is the rotating coordinate frame fixed to the root of the link. A motor is installed on the root of the link. The rotational angle of the motor when the link rotates is denoted by $\theta(t)$.

The position vector $\boldsymbol{r}(x,t)$ of the arbitrary point P in the link at time $t = t$, measured in the $O - XY$ frame shown in figure 1 is expressed by

$$\boldsymbol{r}(x,t) = X(x,t)\boldsymbol{I} + Y(x,t)\boldsymbol{J} \tag{1}$$

Where

$$X(x,t) = x\cos\theta(t) - v(t)\sin\theta(t) \tag{2}$$

$$Y(x,t) = x\sin\theta(t) + v(t)\cos\theta(t) \tag{3}$$

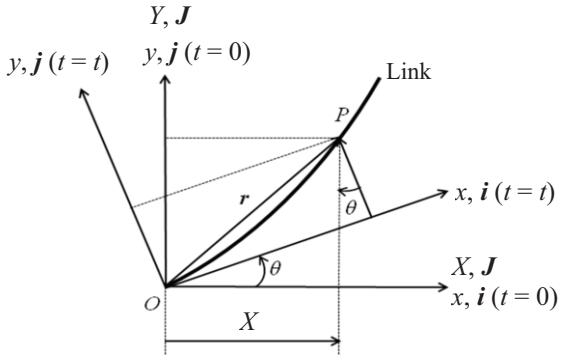

O – XY: Global coordinate frame
O – xy : Rotating coordinate frame

Fig. 1. Position vector of an arbitrary point *P* in the link in the global and rotating coordinate frames

The velocity of *P* is given by

$$\dot{\boldsymbol{r}}(x,t) = \dot{X}(x,t)\boldsymbol{I} + \dot{Y}(x,t)\boldsymbol{J} \tag{4}$$

2.2 Finite-element method

Figure 2 shows the rotating coordinate frame and the link divided by one-dimensional and two-node elements. Then, figure 3 shows the element coordinate frame of the *i-th* element.

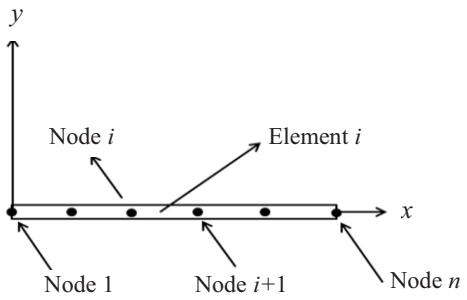

o – xy: Rotating coordinate frame

Fig. 2. Rotating coordinate frame and the link divided by the one-dimensional and two-node elements

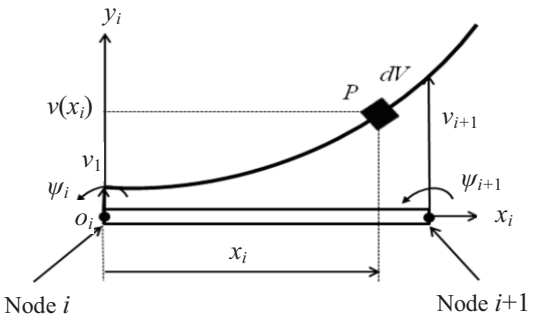

$o_i – x_i\, y_i$: Element coordinate frame of the *i*-th element

Fig. 3. Element coordinate frame of the *i-th* element

Here, there are four boundary conditions together at nodes *i* and (*i*+1) when the one-dimensional and two-node element is used. The four boundary conditions are expressed as nodal vector as follow

$$\boldsymbol{\delta}_i = \{v_i \quad \psi_i \quad v_{i+1} \quad \psi_{i+1}\}^T \tag{5}$$

Then, the hypothesized deformation has four constants as follows [1]

$$v_i = a_1 + a_2 x_i + a_3 {x_i}^2 + a_4 {x_i}^3 \tag{6}$$

The relation between the lateral deformation v_i and the rotational angle ψ_i of the node *i* is given by

$$\psi_i = \frac{\partial v_i}{\partial x_i} \tag{7}$$

Furthermore, from mechanics of materials, the strain of node *i* can be defined by

$$\varepsilon_i = \varepsilon_{x_i} = -y_i \frac{\partial^2 v_i}{\partial {x_i}^2} \tag{8}$$

2.3 Equation of motion

Equation of motion of the *i-th* element is given by

$$\boldsymbol{M}_i \ddot{\boldsymbol{\delta}}_i + \boldsymbol{C}_i \dot{\boldsymbol{\delta}}_i + \left(\boldsymbol{K}_i - \dot{\theta}^2(t)\boldsymbol{M}_i\right)\boldsymbol{\delta}_i = \ddot{\theta}(t)\boldsymbol{f}_i \tag{9}$$

Where $\boldsymbol{M}_i$, $\boldsymbol{C}_i$, $\boldsymbol{K}_i$, $\ddot{\theta}(t)\boldsymbol{f}_i$ are the mass matrix, damping matrix, stiffness matrix and the excitation force generated by the rotation of the motor respectively. The matrices and vector in Eq. (9) are represented as

$$\boldsymbol{M}_i = \frac{\rho_i S_i l_i}{420}\begin{bmatrix} 156 & 22l_i & 54 & -13l_i \\ 22l_i & 4{l_i}^2 & 13l_i & -3{l_i}^2 \\ 54 & 13l_i & 156 & -22l_i \\ -13l_i & -3{l_i}^2 & -22l_i & 4{l_i}^2 \end{bmatrix} \tag{10}$$

$$\boldsymbol{K}_i = \frac{E_i I_{z_i}}{{l_i}^3}\begin{bmatrix} 12 & 6l_i & -12 & 6l_i \\ 6l_i & 4{l_i}^2 & -6l_i & 2{l_i}^2 \\ -12 & -6l_i & 12 & -6l_i \\ 6l_i & 2{l_i}^2 & -6l_i & 4{l_i}^2 \end{bmatrix} \tag{11}$$

$$\boldsymbol{C}_i = \alpha \boldsymbol{K}_i \tag{12}$$

$$\boldsymbol{f}_i^T = \frac{\rho_i S_i l_i}{60}\left\{30l_{1-i} + 9l_i, \quad 5l_{1-i}l_i + 2{l_i}^2, \right. \\ \left. 21l_i, \quad -5l_{1-i}l_i + 3{l_i}^2\right\} \tag{13}$$

The length of the *i-th* element, the length from element 1 to i, and the Rayleigh damping factor are denoted by l_i, l_{1-i}, and α [1] respectively.

Finally, the equation of motion of the system with n elements considering the boundary conditions is given by

$$\boldsymbol{M}_n\ddot{\boldsymbol{\delta}}_n + \boldsymbol{C}_n\dot{\boldsymbol{\delta}}_n + \left(\boldsymbol{K}_n - \dot{\theta}^2(t)\boldsymbol{M}_n\right)\boldsymbol{\delta}_n = \ddot{\theta}(t)\boldsymbol{f}_n \qquad (14)$$

3 VALIDATION OF FORMULATION AND COMPUTATIONAL CODES

3.1 Experimental model

Figure 4 shows the experimental model of the single-link manipulator. The single-link manipulator consists of the flexible aluminum beam, the clamp-part, the servo motor and the base. The single-link is attached to the motor through the clamp-part. The motor is mounted to the base. In the experiments, the motor was operated by an independent motion controller.

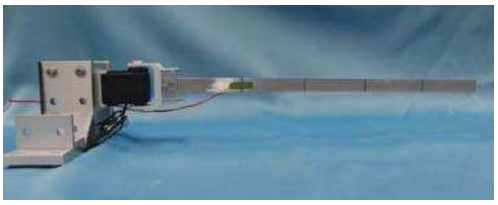

Fig. 4. Experimental model of the single-link manipulator

3.2 Computational models

In this research, we defined and used three types of computational models of the single-link manipulator.

3.2.1 Model Ⅰ

A model of only a single-link manipulator was used as Model Ⅰ. Figure 5.a shows Model Ⅰ. The link and the clamp-part were discretized by 5 elements and 1 element respectively. The clamp-part is much rigid than the link. Therefore Young's modulus of the clamp-part was set in 1,000 times of the link's. A strain gage is bonded to the position of Node 3 of the single-link (0.11 m from the origin).

3.2.2 Model Ⅱ

A model of the single - link manipulator including the couple of piezoelectric actuators was defined as Model Ⅱ. Figure 5.b shows Model Ⅱ. The piezoelectric actuators were bonded to the both surfaces of element 2. The link was discretized by 22 elements. A schematic representation on modeling of the piezoelectric actuators is shown in figure 6. Physical parameters of the single-link model and the piezoelectric actuators are shown in table 1.

The piezoelectric actuator suppresses the vibration of the single-link flexible manipulator by adding moments of force at nodes 2 and 3, M_2 and M_3 to the single-link. The moments of force are generated by applying voltages $\pm E$ to the piezoelectric actuators as shown in figure 6. The relation between the moments of force and the voltages are related by

$$M_{2,3} = \pm d_1 E \qquad (15)$$

Here d_1 is a constant quantity.

Furthermore, the voltage to generate the moments of force is proportional to the strain ε of the single-link due to the vibration. The relation can be expressed as follows

$$\varepsilon = \pm d_2 E \qquad (16)$$

Here d_2 is a constant quantity. Then, d_1 and d_2 will be determined by comparing the calculated results and experimental ones.

Substituting Eq. (16) to Eq. (15) gives

$$M_{2,3} = \pm \frac{d_1}{d_2}\varepsilon \qquad (17)$$

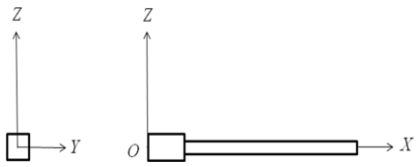

(a) Model Ⅰ: Only single-link

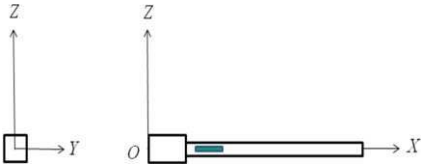

(b) Model Ⅱ: Single-link with actuators

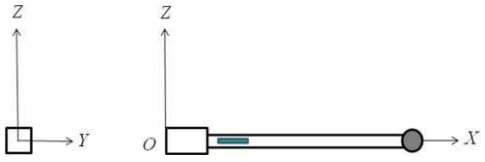

(c) Model Ⅲ: Single-link with actuators and end efector

Fig. 5. Computational models of the single-link manipulator

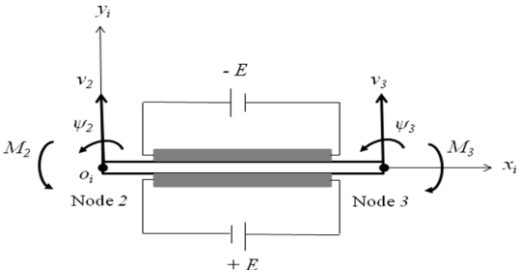

Fig. 6. Modeling piezoelectric actuator

3.2.3 Model Ⅲ

Figure 5.c shows Model Ⅲ that an end effector of a single-link manipulator is considered by adding a concentrated mass to Model Ⅱ. In this case, the equation

of motion of the tip element containing the concentrated mass is given by

$$\begin{aligned}&\left\{\boldsymbol{M}_i+\boldsymbol{M}_{i_{cm}}\right\}\ddot{\boldsymbol{\delta}}_i+\boldsymbol{C}_i\dot{\boldsymbol{\delta}}_i\\&+\left\{\boldsymbol{K}_i-\dot{\theta}^2(t)\left(\boldsymbol{M}_i+\boldsymbol{M}_{i_{cm}}\right)\right\}\boldsymbol{\delta}_i=\ddot{\theta}(t)\left\{\boldsymbol{f}_i+\boldsymbol{f}_{i_{cm}}\right\}\end{aligned}\tag{18}$$

where the vector of $\boldsymbol{f}_{i_{cm}}$ is given by

$$\boldsymbol{f}_{i_{cm}}=-m_c\left\{0\quad 0\quad l_{1-i}+l_i\quad 0\right\}^T\tag{19}$$

Then the concentrated mass matrix $\boldsymbol{M}_{i_{cm}}$ can be expressed as

$$\boldsymbol{M}_{i_{cm}}=\begin{bmatrix}0&0&0&0\\0&0&0&0\\0&0&m_c&0\\0_i&0&0&0\end{bmatrix}\tag{20}$$

Tabel 1. Physical parameters of the single-link and the piezoelectric actuators [2]

l : Total length	m	3.91×10^{-1}
l_l : Length of the link	m	3.50×10^{-1}
l_c : Length of the clamp-part	m	4.10×10^{-2}
l_a : Length of the actuator	m	2.00×10^{-2}
S_l : Cross section area of the link	m^2	1.95×10^{-5}
S_c : Cross section area of the clamp-part	m^2	8.09×10^{-4}
S_a : Cross section area of the actuator	m^2	1.58×10^{-5}
I_{zl} : Cross section area moment of inertia around z-axis of the link	m^4	2.75×10^{-12}
I_{zc} : Cross section area moment of inertia around z-axis of the clamp-part	m^4	3.06×10^{-8}
I_{za} : Cross section area moment of inertia around z-axis of the actuator	m^4	1.61×10^{-11}
E_l : Young's Modulus of the link	GPa	7.03×10^{1}
E_c : Young's Modulus of the clamp-part	GPa	7.00×10^{4}
E_a : Young's Modulus of the actuator	GPa	4.40×10^{1}
ρ_l : Density of the link	kg/m^3	2.68×10^{3}
ρ_c : Density of the clamp-part	kg/m^3	9.50×10^{2}
ρ_a : Density of the actuator	kg/m^3	3.33×10^{3}
α : Damping factor of the link	-	2.50×10^{-4}

3.3 Time history response of free vibration

Experiment on free vibration was conducted using an impulse force as an external one. Figure 7.a shows the experimental time history response of strains ε_e on the free vibration at the same position used in the calculation.

Furthermore, the computational codes on time history response of model I were developed. Figure 7.b shows the calculated strains at Node 3 of Model I under the impulse force.

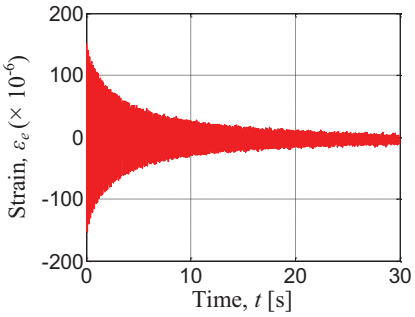

(a) Experimental result at 0.11 m from the origin

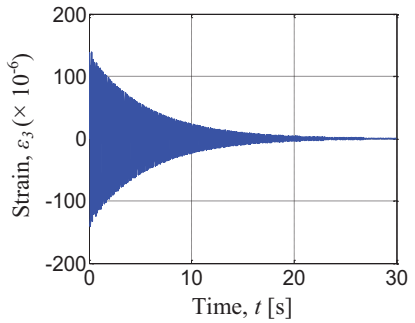

(b) Calculated result at Node 3 of Model I

Fig.7. Time history response of strains on free vibration of the single-link

3.4 FFT (Fast Fourier Transform) processing

Both the experimental and calculated time history responses of free vibration were transferred to their frequencies by FFT processing.

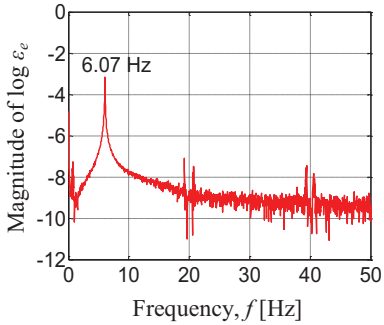

Fig. 8. Experimental natural frequency of the single-link

Figures 8 and 9 show the experimental and calculated natural frequencies of the single-link manipulator, respectively. The experimental first natural frequency, 6.07 Hz well agreed with the calculated one. The second and third experimental natural frequencies could not be measured. However, in the calculation, they could be obtained as 38.00 Hz and 105.40 Hz.

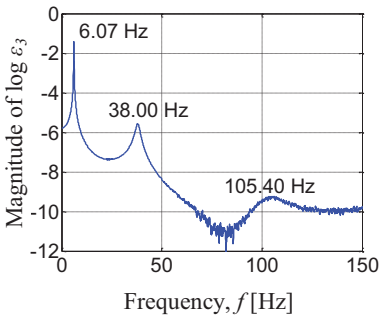

Fig. 9. Calculated natural frequencies of Model I

3.5 Eigenvalues and eigenvectors analysis

The computational codes on eigenvalues - eigenvectors analysis were developed to find natural frequencies and vibration modes. The calculated results for the first, second and third natural frequencies were 6.10 Hz, 38.22 Hz, and 107.19 Hz respectively. The vibration modes of natural frequencies are shown in figure 10.

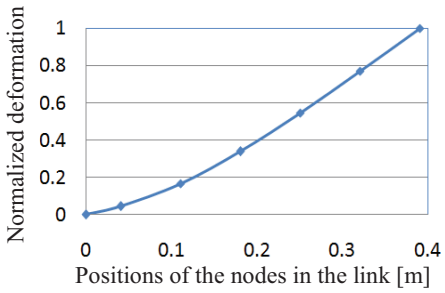

(a) First vibration mode (f_1 = 6.10 Hz)

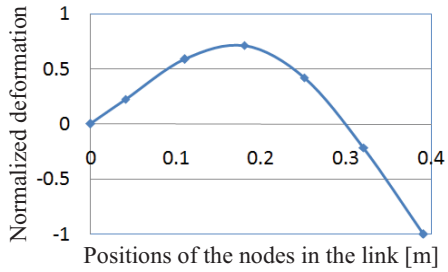

(b) Second vibration mode (f_2 = 38.22 Hz)

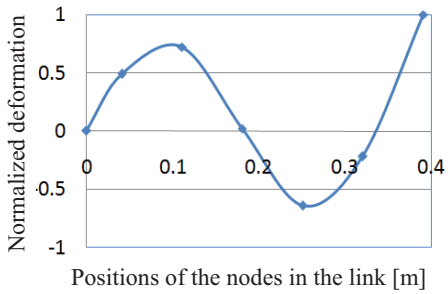

(c) Third vibration mode (f_3 = 107.19 Hz)

Fig. 10. Vibration modes and natural frequencies of Model I

3.6 Time history responses due to the excitation force

Another experiment was conducted to investigate the vibration of the link due to the excitation force generated by rotation of the motor. In the experiment, the motor was rotated by the angle of $\pi/2$ radians (90 degrees) for 2.05 seconds. Figure 11 shows the experimental time history response of strains due to the motor's rotation at the same position in calculation (0.11 m from the origin). Based on figure 11, the angular acceleration of the motor was calculated. Time history response of the motor's acceleration is shown in figure 12. Furthermore, based on figures 11 and 12, the time history response of strains at Node 3 of Model I was calculated as shown in figure 13.

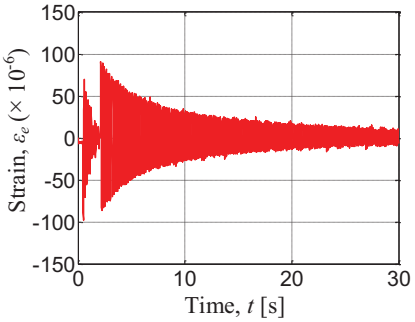

Fig. 11. Experimental time history responses of strains at 0.11 m from the origin of the single-link due to the excitation force generated by the motor's rotation

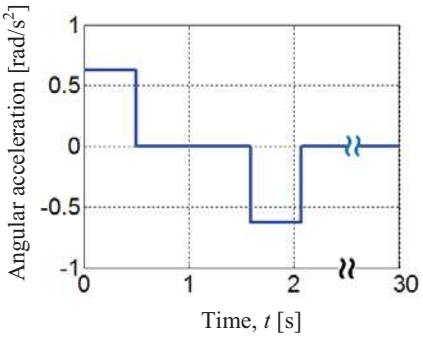

Fig. 12. Time history response of angular acceleration of the motor

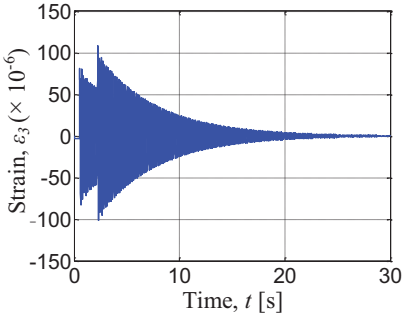

Fig. 13. Calculated time history responses of strains at Node 3 of Model I due to the excitation force generated by the motor's rotation

The above results show the validities of the formulation, computational codes and modeling the flexible single-link manipulator.

4 CONTROL SCHEME AND SIMULATIONS

4.1 Control scheme

A PD (proportional-derivative) controller was designed so that vibration due to motor's rotation of a single-link system can become smaller.

Based on equation (17), the moments of force can be defined in term of the PD controller as follows

$$M_{2,3} = \pm\left\{K_p\left(\varepsilon_{4_d} - \varepsilon_4\right) + K_d \frac{d\left(\varepsilon_{4_d} - \varepsilon_4\right)}{dt}\right\} \tag{21}$$

Furthermore, the equation of motion of the controlled single-link manipulator with n-elements is given by

$$\boldsymbol{M}_n\ddot{\boldsymbol{\delta}}_n + \boldsymbol{C}_n\dot{\boldsymbol{\delta}}_n + \left(\boldsymbol{K}_n - \dot{\theta}^2(t)\boldsymbol{M}_n\right)\boldsymbol{\delta}_n = \ddot{\theta}(t)\boldsymbol{f}_n + \boldsymbol{u}_n(t) \tag{22}$$

where the vector of $\boldsymbol{u}_n(t)$ containing M_2 and M_3 is the control force generated by the actuators to the single-link.

Finally, a feedback control scheme of the single-link is shown in figure 14.

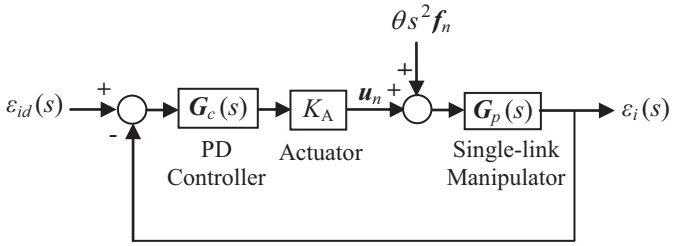

Fig. 14. Block diagram of feedback control of the flexible single-link manipulator

4.2 Calculated results

The time history responses of strains at Node 4 in the controlled system were calculated for Models Ⅱ and Ⅲ under the control scheme as shown in figure 14. The concentrated mass m_c used for Model Ⅲ is 0.01 kg.

Examining several gains of the PD controller leaded to P-gain of 1,000 [Nm/V] and D-gain of 0.058 [Nms/V] as the better ones. Figures 15 and 16 show both the uncontrolled and controlled time history responses for Model Ⅱ and Ⅲ, respectively. They were calculated when the motor rotated by the angle of $\pi/2$ radians (90 degrees). The maximum strains of uncontrolled for Model Ⅱ are 22.80×10^{-6} and the controlled one becomes 9.76×10^{-6}, respectively, as shown in figure 15. The maximum strains of uncontrolled Model Ⅲ are 46.00×10^{-6} and the controlled one becomes 21.40×10^{-6}, respectively, as shown in figure 16. It was verified from these results that the proposed control scheme can effectively suppress the vibration of the flexible single-link manipulator.

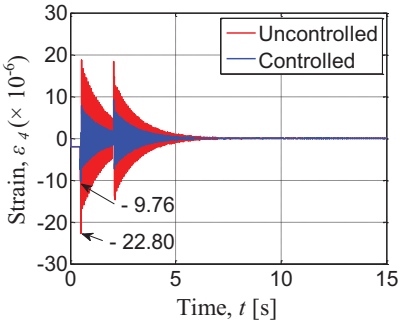

Fig. 15. The calculated time history responses of strains at Node 4 for uncontrolled and controlled model Ⅱ due to the excitation force generated by the motor's rotation (K_p = 1,000 [Nm/V] and K_d = 0.058 [Nms/V])

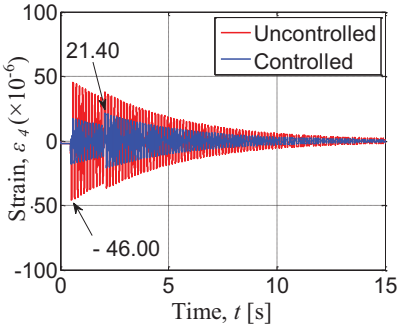

Fig. 16. The calculated time history responses of strains at Node 4 for uncontrolled and controlled model Ⅲ due to the excitation force generated by the motor's rotation (m_c = 0.01 kg, K_p = 1,000 [Nm/V] and K_d = 0.058 [Nms/V])

5 CONCLUSIONS

The equation of motion for the flexible single-link manipulator had been derived using the finite-element method. Computational codes had been developed in order to perform dynamics simulations of the system. Experimental and calculated results on time history responses, natural frequencies and vibration modes show the validities of the formulation, computational codes and modeling of the system. A simple and effective control scheme was designed to suppress the vibration of the system. The calculated results have been revealed that the vibration of the system can be suppressed effectively. The derivative gain used in the calculation is very small compared to proportional gain. Therefore, using a proportional controller will be sufficient for practical applications of the proposed control scheme.

REFERENCES

[1] M. Lalanne, P. Berthier, J. D. Hagopiean , *Mechanical Vibration for Engineers*, John Wiley & Sons Ltd, 1983, pp. 146 -153.

[2] www.mmech.com, *Resin Coated Multilayer Piezoelectric Actuators.*